J. Fluid Mech. (1994), *vol.* 270, *pp.* 251–275

Secondary and tertiary excitation of three-dimensional patterns on a falling film

By H.-C. CHANG†, M. CHENG, E. A. DEMEKHIN‡ AND D. I. KOPELEVICH‡

Department of Chemical Engineering, University of Notre Dame, Notre Dame, IN 46556, USA

(Received 6 June 1993 and in revised form 20 December 1993)

The primary instability of a falling film selectively amplifies two-dimensional noise down-stream over three-dimensional modes with transverse variation. If the initial three-dimensional noise is weak or if it has short wavelengths such that they are effectively damped by the capillary mechanism of the primary instability, our earlier study (Chang *et al.* 1993*a*) showed that the primary instability leads to a weakly nonlinear, nearly sinusoidal γ_1 stationary wave which then undergoes a secondary transition to a strongly nonlinear γ_2 wave with a solitary wave structure. We show here that the primary transition remains in the presence of significant three-dimensional noise but the secondary transition can be replaced by a selective excitation of oblique triad waves which can even include stable primary disturbances. The resulting secondary checkerboard pattern is associated with a subharmonic mode in the streamwise direction. If the initial transverse noise level is low, a secondary transition to a two-dimensional γ_2 solitary wave is followed by a tertiary 'phase instability' dominated by transverse wave crest modulations.

1. Introduction

In many unstable open-flow systems which selectively amplify two-dimensional disturbanes at inception over three-dimensional ones, the evolution towards the final turbulent and fully three-dimensional waves often involves the long duration of two-dimensional waves that are locally stationary, namely they travel at constant speed for a long time without significant variation in their shape. These systems include shear layers (Thomas 1990), bounded Poiseuille flows (Orszag & Kells 1980) and the falling-film instability studied here. The three-dimensional disturbances are then secondary instabilities triggered by finite-amplitude two-dimensional stationary waves. The preferential excitation of the three-dimensional waves suggests that, in contrast to the primary instability which satisfies the analogue of Squire's theorem, three-dimensional secondary disturbances are more unstable than two-dimensional ones. It then becomes a key step in the downstream evolution towards turbulence. The analysis of these secondary transitions to turbulence is simplified by the long lifetimes of the saturated two-dimensional stationary waves beyond the primary instability. This is especially true for the transitions on a falling film at relatively low flow rates (for Reynolds numbers $R < 300$) where the stationary waves are well characterized experimentally. These secondary transitions can be studied by constructing all two-dimensional

† Author to whom all correspondence should be addressed.

‡ Permanent address: Department of Applied Mathematics, Krasnodar Polytechnical Institute, Krasnodar, 350072, Russia.

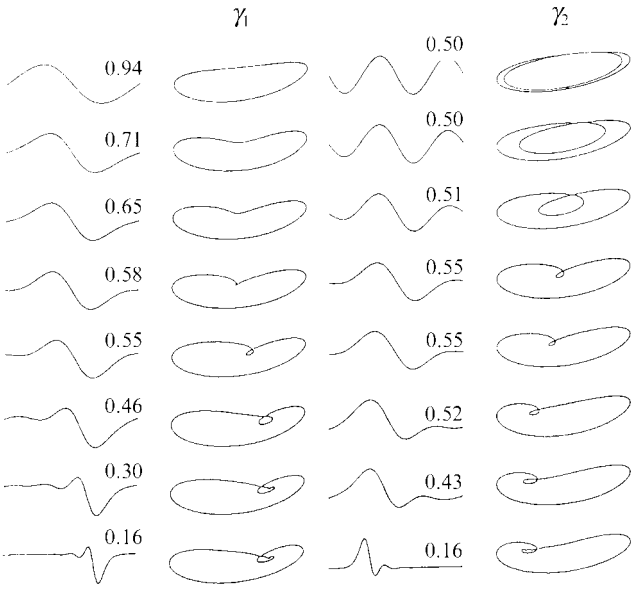

FIGURE 1. The wave profiles and phase-space trajectories of the γ_1 and γ_2 family at small δ. The normalized wavenumber $k = \alpha/\alpha_0$ is also labelled, where α_0 is the neutral wavenumber. The γ_1 family ranges from $k \in (0, 1)$ while the γ_2 family lies within $k \in (0, 0.5)$. The most stable (least unstable) wavemember of the γ_1 family is at $k_s = \alpha_s/\alpha_0 \sim 0.76$ and its wave profile resembles the second γ_1 wave shown. The phase-space trajectories are in the space of (h, h_X, h_{XX}). The solitary wave limit at vanishing k approaches a homoclinic orbit connected to the flat-film fixed point $(1, 0, 0)$, reflecting the fact that all periodic stationary waves, which are closed trajectories in the phase space, arise from a Silnikov global bifurcation of the homoclinic orbit. The amplitude of the wave and closed trajectories increases with decreasing k but they are not drawn to scale.

stationary waves and studying their stability to two-dimensional and three-dimensional disturbances. The results determine not only which two-dimensional waves are selected beyond the primary transition but also what kind of secondary three-dimensional patterns are generated subsequently.

For a low-Reynolds-number falling film, the initial filtering of small-amplitude transverse variation is due to the stabilizing effect of surface tension when inertia is small. As a result, two-dimensional stationary waves are very pronounced in wave transition on falling films (Chang 1994). These stationary waves have now been exhaustively constructed and favourably compared to observed ones (Chang, Demekhin & Kopelevich 1993*a*). Under most conditions, two families of periodic stationary waves, γ_1 and γ_2, are involved in the transition. For vertical or nearly vertical films, the γ_1 waves travel slower than the linear phase speed, which is three times the average fluid velocity at inception, while the γ_2 waves travel much faster than the phase speed of an infinitesimally small wave of the same wavelength. The wavenumber of the γ_1 family extends from α_0, the neutral wavenumber, to the solitary wave limit of zero. However, from our stability analysis, the wave member most stable (or least unstable) to two-dimensional disturbances is at $\alpha_s \sim 0.8\alpha_0$, which is slightly shorter than the linearly maximum growing mode at $\alpha_m \sim \alpha_0/\sqrt{2}$. Near the critical Reynolds number, this specific wave member at α_s is stable to two-dimensional disturbances but, sufficiently far from criticality, it becomes merely the least unstable. Since its wavenumber is close to the neutral value of α_0, its amplitude is small and its shape is nearly sinusoidal with only a small overtone content. It can hence be estimated

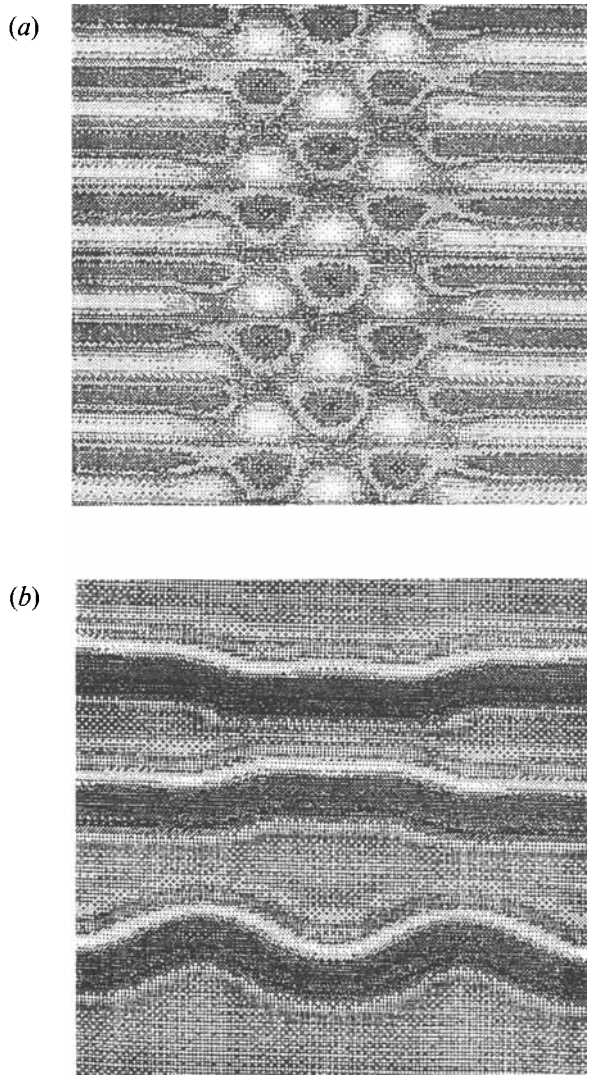

FIGURE 2. The two dominant three-dimensional patterns: (*a*) the herringbone pattern with a checkerboard middle strip; (*b*) the crest-modulating phase instability. The white regions represent crests and black regions valleys. The *x*- and *y*-axes in this figure correspond to the transverse and streamwise directions, respectively.

by a weakly nonlinear formalism like the Stuart–Landau expansion from the neutral curve (Chang 1994). The γ_2 wave branch, on the other hand, begins at a wavenumber of $\alpha_2 \sim 0.5\alpha_0$ and extends to zero wavenumber. They are hence much larger in amplitude with a large Fourier content. Their shapes resemble localized solitary waves. These strongly nonlinear waves cannot be analysed with weakly nonlinear bifurcation theories and are best described by a Silnikov global bifurcation analysis of a homoclinic orbit (Chang, Demekhin & Kopelevich 1993*b*). Also unlike the γ_1 branch, the γ_2 branch has infinitely many segments that stable to two-dimensional disturbances even far from criticality. Our earlier two-dimensional simulation (Chang *et al.* 1993*a*) indicates that waves at inception first evolve towards the nearly sinusoidal α_s wave on γ_1 and then towards a stable nearly solitary wave on γ_2. The waves then stay at one

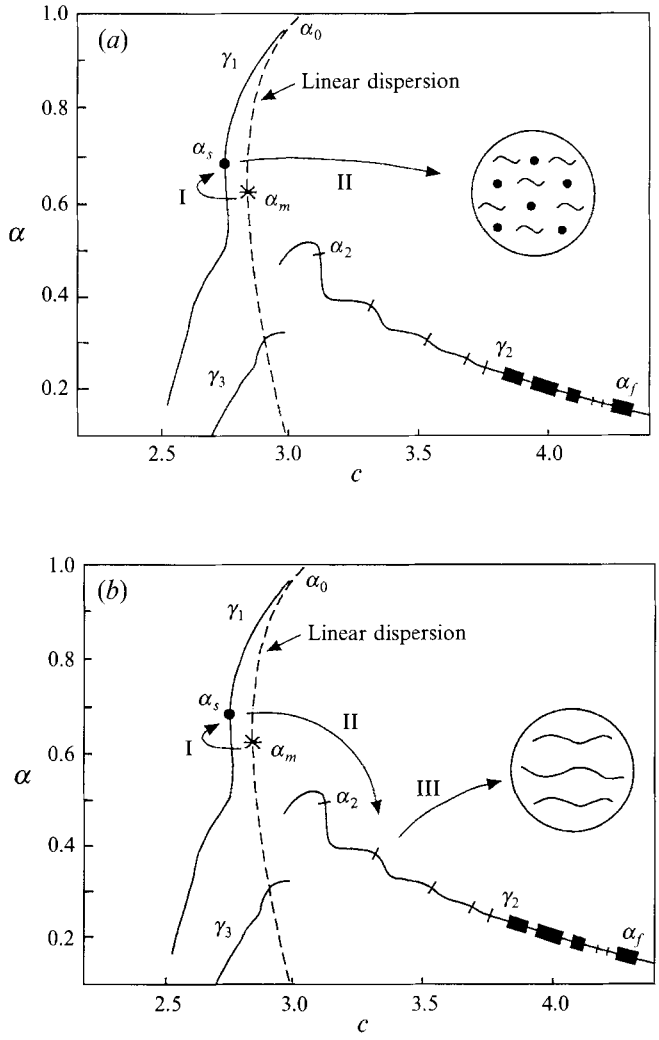

FIGURE 3. The two speculated transitions to three-dimensional patterns for $\delta = 0.062$. (*a*) The checkerboard pattern appears when there is significant transverse variation initially. Otherwise, (*b*), transition to a γ_2 wave is followed by crest modulation. The wave members on γ_2 that are stable to two-dimensional waves are marked by thick segments.

of these locally stable γ_2 waves indefinitely unless persistent large-amplitude noise is present to push the system out of its domain of attraction. There is a lower bound α_f for the wavenumber of γ_2 waves stable to two-dimensional disturbances. Periodic forcing to generate γ_2 waves below α_f has resulted in chaotic two-dimensional wave patterns in several experiments (Alekseenko, Nakoryakov & Pokusaev 1985; Liu, Paul & Gollub 1993). Representative wave profiles of the γ_1 wave family, including the nearly sinusoidal one at α_s, and the γ_2 wave family, including the long stable nearly solitary waves whose distinctive humps have sloping backs and steeper fronts relaxed by small 'bow' waves, are shown in figure 1. We note from the figure that there is near symmetry between the near-solitary waves of the γ_1 and γ_2 families. We have shown that (Chang *et al.* 1993*a*), for near critical conditions, they are related by an inversion (wave height $\rightarrow$ negative height) and a reflection ($x \rightarrow -x$). However, the inverted near-

solitary waves, analogous to negative solitons, of the γ_1 waves are unstable for vertical films and have never been observed. The positive near-solitary waves of the γ_2 wave, in contrast, are very stable far from criticality and they dominate the interfacial structure during wave evolution.

If there is a significant amount of three-dimensional disturbances, the transition scenario can be quite different. In a recent numerical analysis of low-Reynolds-number falling films, Joo & Davis (1992) suggested that all γ_1 stationary waves are unstable to three-dimensional disturbances. This is confirmed by our recent stability analysis of the γ_1 and γ_2 waves for much larger Reynolds numbers (Chang *et al.* 1993*a*). Experimental studies by Liu *et al.* (1992) for an inclined film have also shown that, at sufficiently large distance downstream, two-dimensional stationary waves will trigger two types of secondary three-dimensional wave pattern – a herringbone pattern and a wavering-crest 'phase' instability. The former resembles a middle strip of checkerboard three-dimensional pattern flanked by strips of two-dimensional crests with approximately one-half the streamwise wavelength of the middle strip (see our reconstruction in figure 2*a*). In the experiments, the 'side bones' bow slightly because of boundary retardation effects to give the herringbone appearance. The second three-dimensional pattern involves a long-wave transverse variation which distorts the crests but does not pinch them off initially since the streamwise disturbance is negligible in amplitude compared to the wave crest (figure 2*b*). (Pinch-off will occur eventually if the lateral modulations are sufficiently large to bridge two neighbouring crests.) We shall show in this paper that the checkerboard in the middle of the herringbone pattern is excited by the γ_1 waves near α_s while the phase instability is characteristic of three-dimensional waves excited by the γ_2 waves. We shall establish that the primary transition to the α_s wave of the γ_1 family is relatively insensitive to the noise characteristics owing to the filtering effect of the primary instability. Secondary transitions from the α_s wave, however, are highly sensitive to the level of three-dimensional noise. The checkerboard transition ensues if there is sufficient disturbance in the transverse direction. Otherwise, a nearly two-dimensional evolution towards a γ_2 wave occurs followed by excitation of transverse disturbances in the form of the phase instability (see figure 3).

2. Primary linear stability and stationary waves

In our earlier studies (Chang *et al.* 1993*a*; Chang 1994), we have shown that, since the characteristic lengthscale in the normal direction y is much shorter than those in the down-stream x and transverse z directions, the equation of motion for a relatively low-Reynolds-number film ($R < 300$) can be simplified by a 'boundary-layer' approximation which neglects the $\partial/\partial x$ and $\partial/\partial z$ terms relative to the $\partial/\partial y$ term. We have shown that this simplification is an excellent one, as far as the linear stability analysis and the stationary wave profiles are concerned, for most fluids. Yet it offers a significant numerical advantage because the omitted terms tend to induce numerical instability and yield complex terms in the interfacial conditions (Chang, Demekhin & Kopelevich 1993*c*). Scaling the streamwise and transverse velocities by $\langle u\rangle$ and the smaller y-component by $\langle u\rangle/\kappa$, y by h_N and (x, z) by κh_N, and time by $\kappa h_N/\langle u\rangle$, where $\langle u\rangle = gh_N^2/3\nu$ is the average velocity, h_N is the Nusselt film thickness for the flat film and

$$\left.\begin{aligned} &\kappa = \gamma/3^{\frac{2}{3}}R^{\frac{2}{3}} = (\tfrac{1}{3}WR)^{\frac{1}{3}} = (\sigma/\rho g h_N^2)^{\frac{1}{3}}, \\ &\gamma = \sigma/\rho\nu^{\frac{4}{3}}g^{\frac{1}{3}}, \quad R = \langle u\rangle h_N/\nu, \quad W = \sigma/\rho\langle u\rangle^2 h_N \end{aligned}\right\} \tag{1}$$

are the scaling parameter, Kapitza, Reynolds and Weber numbers where g, ν, σ, ρ are

gravitational acceleration, the liquid kinematic viscosity, surface tension and density, one obtains the following boundary-layer equations:

$$\frac{\partial u}{\partial t}+\frac{\partial u^2}{\partial x}+\frac{\partial}{\partial y}(uv)+\frac{\partial (wu)}{\partial z}=\frac{1}{5\delta}\left(h_{xxx}+h_{xzz}+\frac{1}{3}\frac{\partial^2 u}{\partial y^2}+1\right), \tag{2a}$$

$$\frac{\partial w}{\partial t}+\frac{\partial}{\partial x}(uw)+\frac{\partial}{\partial y}(vw)+\frac{\partial w^2}{\partial z}=\frac{1}{5\delta}\left(h_{xxz}+h_{zzz}+\frac{1}{3}\frac{\partial^2 w}{\partial y^2}\right), \tag{2b}$$

which are coupled to the continuity and kinematic equations

$$\frac{\partial u}{\partial x}+\frac{\partial v}{\partial y}+\frac{\partial w}{\partial z}=0, \tag{2c}$$

$$\frac{\partial h}{\partial t}+\frac{\partial}{\partial x}\int_0^h u\,\mathrm{d}y+\frac{\partial}{\partial z}\int_0^h w\,\mathrm{d}y=0, \tag{2d}$$

with boundary conditions

$$y=h(x,z,t),\quad \frac{\partial u}{\partial y}=\frac{\partial w}{\partial y}=0, \tag{2e}$$

$$y=0,\quad u=v=w=0. \tag{2f}$$

The long-wave expansion of the boundary-layer approximation has been invoked to yield (2*e*). The lone parameter that appears in the above equation is

$$\delta=R^{\frac{11}{9}}/5\gamma^{\frac{1}{3}}3^{\frac{7}{9}}, \tag{3}$$

which is a normalized Reynolds number that measures ratio of inertia to surface tension. The Navier–Stokes equation is parameterized by two parameters, R and W. The boundary-layer approximation hence yields the additional advantage that the number of parameters is reduced to one.

Using the same expansion as in our earlier analysis of the two-dimensional problem, it can be shown that a primary disturbance to the Nusselt-flat-film basic state with a normal mode of the form $\exp \mathrm{i}(\alpha x+\beta z-\alpha ct)$ yields the following relationship for the neutral curve ($c_i=0$) in the limit of small δ:

$$c=3,\quad 18\alpha^2\delta=(\alpha^2+\beta^2)^2. \tag{4}$$

This neutral curve reduces to the two-dimensional version derived earlier (Chang *et al.* 1993*a*):

$$c_0=3,\quad \alpha_0^2=18\delta, \tag{5}$$

where α_0 is the neutral wavebumber for two-dimensional disturbances with zero growth rate and c_0 is the phase speed at the neutral wavenumber. The growth rate αc_i and the neutral curves are sketched in figure 4. It is clear that the primary three-dimensional disturbances are more stable than two-dimensional disturbances ($\beta=0$) in an analogue of Squire's theorem. This is then the linear filtering mechanism that tends to filter away transverse variation during inception.

In the limit when δ approaches zero (near criticality limit, see figure 4) such that both α and β of the unstable linear modes become small, of $O(\delta^{\frac{1}{2}})$, one can further simplify the equation of motion in the low-Reynolds-number limit by using the stretching transformations

$$H=\tfrac{3}{2}(h-1)/\alpha_0^3,\quad X=(x-3t)\alpha_0,\quad Z=z\alpha_0\quad\text{and}\quad T=\alpha_0^2 t,$$

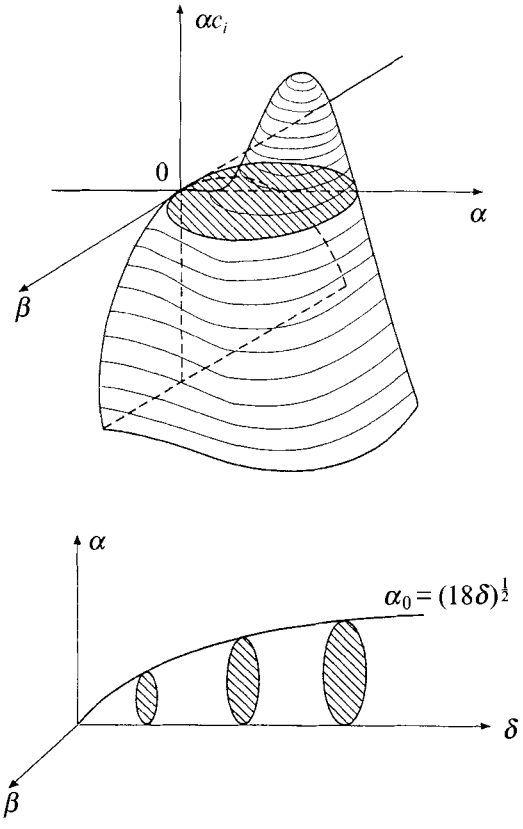

FIGURE 4. The primary growth rate and neutral curves of the boundary-layer equations.

where $\alpha_0 = (18\delta)^{\frac{1}{2}}$ is the neutral wavenumber of two-dimensional disturbances in (5), to yield the two-dimensional Kuramoto–Sivashinsky (KS) equation first derived by Nepomnyaschy (1974*a*):

$$H_T + 4HH_X + H_{XX} + \left(\frac{\partial^2}{\partial X^2} + \frac{\partial^2}{\partial Z^2}\right)^2 H = 0, \tag{6}$$

which has even absorbed the lone parameter δ of the boundary-layer equation. The stretching in space in the above derivation came from the consideration that the unstable wavenumbers are of $O(\alpha_0)$ or $O(\delta^{\frac{1}{2}})$ while the stretching in time comes from the linear growth which is of $O(\delta)$. These are the natural scalings. However, the $\delta^{\frac{3}{2}}$ scaling in the amplitude restricts the Kuramoto–Sivashinsky equation to small-amplitude waves of the prescribed order. Large-amplitude wave solutions of (6) are not physically pertinent. Nevertheless, if one is cognizant that (6) is only valid at $\delta \ll 1$, namely near criticality, and small amplitudes, the KS equation can still be a welcome substitute for the full Navier–Stokes equation or the boundary-layer equation (2) since it is so simple (Chang 1993). We shall use the KS equation to establish the excitation of the checkerboard pattern by small-amplitude two-dimensional γ_1 waves at low δ.

One can extend the amplitude limitation of the KS equation by deriving 'strongly non-linear' evolution equations of the type first derived by Benney (1966) at small δ. However, since there are actually two expansions – one is the long-wave expansion which can be derived by expanding in the film parameter ϵ, which is equivalent to α_0

in (5), or $1/\kappa$ in (1) (see Chang 1933) and one is the small-amplitude expansion – it is quite questionable that one can carry out the expansion in amplitude to all orders while truncating the long-wave expansion at a low order as in the derivation of the strongly nonlinear evolution equation. The two expansion parameters are related but their relative order cannot be assigned *a priori*. It is hence not surprising that the strongly nonlinear evolution equation often yields finite-time blow-up solutions (Pumir, Manneville & Pomeau 1983; Demekhin, Kaplan & Shkadov 1987; Joo, Davis & Bankov 1991; Rosenau, Oron & Hyman 1992). Such solutions arise because physically impertinent large-amplitude waves are tolerated by the strongly nonlinear equations. This can be a serious drawback since these impertinent solutions may camouflage the true evolution. For example, although Joo & Davis (1992) suspected that streamwise subharmonic secondary instabilities are important, they were unable to extend their integration domain to investigate this instability. Attempts to do this led to blow-up solutions which have never been observed at low Reynolds numbers. This is consistent with the observation that the strongly nonlinear equation omits certain important higher-order terms in the long-wave expansion that are not negligible at large amplitudes. Recently, Salamon, Armstrong & Brown (1994) have shown conclusively that the strongly nonlinear equations yield qualitatively incorrect large-amplitude stationary wave solutions. In contrast, the weakly nonlinear KS equation yields the correct description for small-amplitude waves but it is not suitable for large waves. The only realistic simplification of the Navier–Stokes equation is then the boundary-layer equation (2) which seems to capture all correct long-wave evolution and does not exhibit blow-up.

It should also be mentioned that the primary instability described above is a convective one (Joo & Davis 1992), and one should also determine the spatial amplification rate instead of the temporal one shown in figure 4. The formation of saturated waves due to the primary instability is then a noise-driven transition that should be studied with a spatial formulation. The secondary instability of these saturated waves downstream can also be convective (Liu *et al.* 1993). The actual amplification rate and the evolution of the disturbances are quite distinct for absolute and convective primary and secondary instabilities. However, whether the Nusselt flat film and the saturated stationary waves are stable or unstable, the most unstable primary and secondary disturbances are identical in both formulations. In other words, the stability assignment and the wave pattern at onset can be obtained from a temporal formulation. Since it is still numerically formidable to integrate the three-dimensional boundary-layer equation in a large domain to resolve the full convective evolution, we shall study the primary and secondary instabilities with a temporal formulation using periodic boundary conditions. Consequently, while the stability assignment and the dominant patterns that appear at onset are correctly deciphered for both the primary and secondary instabilities, the subsequent evolution to 'turbulence' cannot be captured with quantitative precision by the present formulation. In particular, wave patterns in a convectively unstable system are driven by the noise at the inlet while a temporal formulation transfers this dependence to the initial condition. Consequently, quantitative correlation of the eventual turbulent fluctuation with the persistent inlet noise cannot be analysed with the present approach even though the correlation is expected to exist owing to the nature of convective instability.

To analyse the secondary stability of the saturated stationary waves, we need to construct the waves numerically. In the earlier paper (Chang *et al.* 1993*a*), we have confirmed that the convectively unstable primary instability yields two-dimensional periodic stationary waves downstream that propagate over a long distance without

significant changes in speed and shape. We have hence constructed all such stationary waves for the boundary-layer equation and favourably compared their profiles, speeds and wavelengths to measured ones. There are two pertinent families of stationary waves, γ_1 and γ_2, each parameterized by either the wave speed c or the wavenumber α (see figures 1 and 3). The first family is slower than the neutral wave speed $c_0 = 3$ of (5) and the second one is faster. The two families are shown in figure 3 for $\delta = 0.062$, corresponding to water at $R \sim 5$. The fast γ_2 family lies below $\alpha_2 \sim 0.5\alpha_0$ while the slow γ_1 family extends from the neutral wavenumber α_0 to the solitary wave limit $\alpha \to 0$. The amplitude of the γ_1 family increases with decreasing wavenumber and it vanishes at α_0, namely it bifurcates supercritically from α_0. (The wave profiles in figure 1 are drawn with different scales.) Consequently, at low δ, the near-neutral waves on γ_1 can be approximated by a weakly nonlinear expansion of the stationary version of the KS equation:

$$H^*_{XXX} + H^*_X + 2(H^*)^2 = Q, \quad \langle H^* \rangle = 0, \tag{7a, b}$$

where $\langle \cdot \rangle$ denotes averaging over one wavelength, H^* is the stationary wave solution and $Q = \langle 2(H^*)^2 \rangle$ is the deviation flux. We have also imposed in (7) that the small-amplitude solutions of the KS equation near the neutral curve are standing waves. They correspond to travelling waves with speed $c = 3$, three times the average velocity in the laboratory frame, since the KS equation is valid in a moving frame. Using a two-mode expansion,

$$H^* \sim H_k \sin kX + H_{2k} \sin 2kX, \tag{8a}$$

one can easily show that

$$H_k^2 = k^2(4k^2-1)(1-k^2) = 2k(1-4k^2)H_{2k} \tag{8b}$$

and

$$H_{2k} = \tfrac{1}{2}k(k^2-1) \sim O(H_k^2) \ll H_k. \tag{8c}$$

The out-of-phase term $\cos 2kX$ vanishes exactly in (8*a*) since the KS equation is non-dispersive (Cheng & Chang 1990) and the overtone excited is in phase with the fundamental. The normalized wavenumber $k = \alpha/\alpha_0$ is the normalized wavenumber of the original equation (2). The dependence of α_0 on δ and the relationship $H = 3(h-1)/2\alpha_0^3$ also yield the dependence of the original amplitude h on both α and δ. It is, however, far more convenient for our purpose to express it in the stretched variables of the KS equation. In (8*a*), we have fixed the 'phase' of $H^*(x)$ by stipulating that $H(0) = 0$. A more general formulation using periodic boundary conditions would yield

$$H^* \sim A_k \mathrm{e}^{\mathrm{i}kX} + A_{2k} \mathrm{e}^{\mathrm{i}2kX} + \text{c.c.}, \tag{9a}$$

where

$$A_k = -\tfrac{1}{2}\mathrm{i}H_k, \quad |A_k|^2 = \tfrac{1}{4}k^2(4k^2-1)(1-k^2) = \tfrac{1}{4}H_k^2 \tag{9b}$$

$$A_{2k} = -\tfrac{1}{2}\mathrm{i}H_{2k}, \quad |A_{2k}|^2 = \tfrac{1}{4}H_{2k}^2, \tag{9c}$$

where the complex amplitudes A_k and A_{2k} are purely imaginary owing to the stipulation that H^* vanishes at the origin.

3. Stability of the stationary waves

Because the near-neutral γ_1 waves have small amplitudes, $H_k \sim A_k \ll 1$, and are nearly monochromatic, $H_{2k} \sim O(H_k^2)$ and $A_{2k} \sim O(A_k^2)$, they can be approximated by the weakly nonlinear theory that leads to (8) and (9). Likewise, their stability to two- and three-dimensional disturbances can also be discerned with a similar expansion. We

demonstrate this first with a streamwise stability analysis of the KS stationary waves H^* in (8a) and (9). Carrying out a Fourier expansion of H in X,

$$H \sim \int \mathrm{d}k\, A_k(T)\, \mathrm{e}^{\mathrm{i}kX} + \text{c.c.}, \tag{10}$$

where A_k is the complex amplitude and A_0 is identically zero due to the constant-thickness formulation, and substituting the expansion into the one-dimensional version of the KS equaton in (6), one can invoke the resonant conditions for a specific fundamental amplitude $A_k(T)$

$$k \pm l \pm m = 0 \quad \text{quadratic interaction},$$

$$k \pm l \pm m \pm n = 0 \quad \text{cubic interaction},$$

to select only a discrete subset of the wavenumber line and obtain a set of cubic amplitude equations for these discrete amplitudes. Even though the original equation only possesses quadratic nonlinearities, the amplitude equations exhibit higher-order nonlinear interaction because of the contribution of higher stable harmonics (Cheng & Chang 1990). In particular, if one considers the evolution of a purely periodic wave described by a specific fundamental Fourier mode A_k, which is unaffected by modes other than the overtones of k, the evolution is described by the Stuart–Landau equation

$$\dot{A}_k = \lambda_k A_k - \sigma_k |A_k|^2 A_k, \tag{11}$$

where $\lambda_k = \lambda(k) = k^2 - k^4$ is the linear growth rate of the fundamental and the overdot denotes time derivative with respect to T. The Landau constant can be shown to be (Cheng & Chang 1990)

$$\sigma_k = -16k^2/\lambda_{2k} > 0 \tag{12}$$

for the KS equation, representing the interaction between the fundamental k and the first overtone $2k$. Hence, the saturated stationary wave for this supercritical mode has an amplitude given by A_k of H^* in (9b). However, (11) also allows us to study the stability of H^* to streamwise disturbances that are overtones of k by linearizing (11) about H^* to yield the secondary overtone growth rate

$$d_1 = -2\lambda_k < 0, \tag{13}$$

and hence all nearly neutral stationary waves H^* of the KS equation are stable to their overtone streamwise disturbance. The only secondary excitation of streamwise disturbances hence arises from interaction with modes that are not overtones of k. If we linearize all these terms about H^* in the A_k fundamental amplitude equation, we find that the terms in (11) which involve only the fundamental, are the only ones that survive. Consequently, the fundamental amplitude equation does not have to be considered in linear non-overtone secondary instabilities. This is demonstrated in our earlier analysis of streamwise sideband (Cheng & Chang 1990) and subharmonic (Cheng & Chang 1992) instabilities. We can hence focus on the dominant non-overtone modes that destabilize H^*. Consider one such mode, A_m, such that m is not an integer multiple of k; we examine the nonlinear terms in the amplitude equation of A_m which involve A_k but are linear in the modes that are not overtones of A_k since we are only interested in the dominant secondary instability, namely linear secondary instability of H^*. These terms can be determined from the resonant conditions to be $A_k \bar{A}_{k-m}$, $\bar{A}_k A_{m+k}$,

$|A_k|^2 A_m$ and $A_k^2 \bar{A}_{2k-m}$ where bar denotes complex conjugate. These quadratic and cubic terms, along with the linear term A_m, are the dominant terms in the A_m amplitude equation during the secondary instability of A_k. The modes which participate in the secondary instability of the fundamental $H^* \sim A_k e^{ikX}$ are then a one-parameter family of quartets $\{A_m, A_{k-m}, A_{k+m}, A_{2k-m}\}$, parameterized by the index m, and possibly their complex conjugates. Because of our notation, m can be restricted to the interval $[0, \frac{1}{2}k]$ since A_{k+m} for $k > m > \frac{1}{2}k$, is identical to $A_{2k-(k-m)}$ when $k-m$ is smaller than $\frac{1}{2}k$. Similar arguments apply for $-k < m < -\frac{1}{2}k$ and for $|m|$ larger than k. The case $m = \frac{1}{2}k$ is the subharmonic instability (Cheng & Chang 1992) and the case $m \ll k$ corresponds to the sideband instability (Cheng & Chang 1990) we studied earlier. Here, we shall refer to all m strictly less than $\frac{1}{2}k$ as a sideband instability. The subharmonic and sideband instabilities are hence the dominant instabilities of a small-amplitude periodic stationary wave. The present sideband instability is distinct from the earlier one, or from the classical Eckhaus theory, in that the 'low' mode A_m in the previous analysis was stipulated to be linearly stable. This is not true for the falling film as is evident from the growth rates in figure 4.

Having identified the two-dimensional wave quartet $\{A_m, A_{k\pm m}, A_{2k-m}\}$ that is responsible for the destabilization of a fundamental stationary wave A_k with wavenumber k, we can carry out a five-mode expansion of the KS equation (6):

$$H \sim A_k e^{ikX} + A_m e^{imX} + A_{k+m} e^{i(k+m)X} + A_{k-m} e^{i(k-m)X} + A_{2k-m} e^{i(2k-m)X} + \text{c.c.}$$

Since the fundamental A_k is not important in its own destabilization, one obtains the following leading-order amplitude equation for the quartet:

$$\dot{A}_m = \lambda_m A_m - 4imA_{k-m} A_k - 4imA_k A_{k+m}, \tag{14a}$$

$$\dot{A}_{k-m} = \lambda_{k-m} A_{k-m} - 4i(k-m) A_m A_k - 4i(k-m) A_k A_{2k-m}, \tag{14b}$$

$$\dot{A}_{k+m} = \lambda_{k+m} A_{k+m} - 4i(k+m) A_k A_m, \tag{14c}$$

$$\dot{A}_{2k-m} = \lambda_{2k-m} A_{2k-m} - 4i(2k-m) A_k A_{k-m}. \tag{14d}$$

(See Cheng & Chang 1990, 1992 for the evaluation of the interaction coefficients from Centre Manifold theory.) The streamwise primary growth rate can be easily obtained from (6):

$$\lambda_k = \lambda(k) = k^2 - k^4. \tag{15}$$

Some important information can immediately be extracted from (14) without further analysis. For a vanishingly small stationary wave A_k with the neutral wavenumber $k = 1$, whose amplitude vanishes as is evident from (9*b*), (14) indicates that the most unstable secondary sideband mode is A_{k-m} whose growth rate is the primary growth rate λ_{k-m}. Consequently, since the primary growth rate has a maximum at $k_m = 1/\sqrt{2}$, the most unstable sideband mode of a vanishingly small stationary wave at the neutral wavenumber $k = 1$ or $\alpha = \alpha_0$ is at

$$m_0 = 1 - 1/\sqrt{2}, \tag{16}$$

with the secondary sideband growth rate

$$d_{\pm}^0 = d_{\pm}(m_0) = \lambda(1/\sqrt{2}) = \tfrac{1}{4}. \tag{17}$$

It also clearly shows that all near-neutral stationary waves are unstable to the sideband

instability. In contrast, we shall show that the same argument yields the limiting secondary subharmonic growth rate of a fundamental wave at the neutral curve to be

$$d_{\frac{1}{2}}^0 = \lambda_{\frac{1}{2}} = \tfrac{3}{16}. \tag{18}$$

It is then clear that there is a segment of the γ_1 stationary waves near the neutral curve whose dominant secondary instability is the sideband instability.

As one moves away from the neutral curve ($k = 1$), however, the subharmonic instability will replace the sideband instability as the more dominant secondary disturbance. We establish this by examining the secondary growth rate of any fundamental wave with respect to a nearly subharmonic quarter parameterized by $m = k(\frac{1}{2}-\epsilon)$ with $\epsilon \ll 1$. In particular, we will show that

$$d_{\frac{1}{2}-\epsilon} < d_{\frac{1}{2}} \tag{19}$$

for stationary waves exceeding a critical amplitude which, from (9*b*), corresponds to a critical distance from the neutral curve at $k = k_c < 1$. The secondary growth rate $d_{\frac{1}{2}-\epsilon}$ represents a sideband growth rate with m slightly less than $\frac{1}{2}$. In this range of m, A_{k+m} and A_{2k-m} are stable modes and we can use the Centre Manifold projections from (14*c*) and (14*d*) to determine how these slave modes are 'adiabatically' coupled to the dominant master modes,

$$A_{k+m} \sim \frac{6\mathrm{i}kA_k A_m}{\lambda_{3k/2}-\lambda_{k/2}}, \quad A_{2k-m} \sim \frac{6\mathrm{i}kA_k A_{k-m}}{\lambda_{3k/2}-\lambda_{k/2}}, \tag{20a, b}$$

where the nonlinear coefficients are evaluated at $m = \frac{1}{2}k$ since $\epsilon \ll 1$. Substituting (20) into (14*a*) and (14*b*), we obtain the dominant amplitude equations for $m \sim \frac{1}{2}$:

$$\dot{A}_m = \lambda_m A_m - 4\mathrm{i}mA_k \bar{A}_{k-m} + 12k^2|A_k|^2 A_m/(\lambda_{3k/2}-\lambda_{k/2}), \tag{21a}$$

$$\dot{A}_{k-m} = \lambda_{k-m} A_{k-m} - 4\mathrm{i}(k-m) A_k \bar{A}_m + 12k^2|A_k|^2 A_{k-m}/(\lambda_{3k/2}-\lambda_{k/2}), \tag{21b}$$

where the cubic terms obviously arise from the Centre Manifold projection since the original KS equation only has quadratic nonlinearity. Equation (21) can be written as

$$\begin{pmatrix} \dot{A} \\ \dot{\bar{A}}_{k-m} \end{pmatrix} = \boldsymbol{J} \begin{pmatrix} A_m \\ \bar{A}_{k-m} \end{pmatrix}, \tag{22}$$

where the Jacobian for the secondary evolution is

$$\boldsymbol{J} = \begin{bmatrix} \lambda_m + \dfrac{12k^2|A_k|^2}{\lambda_{3k/2}-\lambda_{k/2}} & -4\mathrm{i}mA_k \\ 4\mathrm{i}(k-m)\bar{A}_k & \lambda_{k-m} + \dfrac{12k^2|A_k|^2}{\lambda_{3k/2}-\lambda_{k/2}} \end{bmatrix}, \tag{23}$$

which is a function of the fundamental wavenumber k and the sideband interval $m = k(\frac{1}{2}-\epsilon)$: $\boldsymbol{J} = \boldsymbol{J}(k, m) = \boldsymbol{J}(k, \epsilon)$. Since, from (9*b*), $|A_k|^2 \sim O(1-k)$ which is small, this Jacobian is a function of the two small parameters $|A_k|$ and ϵ. A simple expansion of the eigenvalue of $\boldsymbol{J}$ yields

$$d_{\frac{1}{2}-\epsilon} \sim d_{\frac{1}{2}} + (\epsilon k)^2 \left[\beta + \frac{\alpha^2 - 16|A_k|^2}{4k|A_k|}\right] \tag{24}$$

to leading order, where

$$d_{\frac{1}{2}} = d(k, \epsilon = 0) = \lambda_{k/2} + 2k|A_k| + \frac{12|A_k|^2}{2-5k^2} \tag{25}$$

is the subharmonic secondary growth rate, and

$$\alpha = \frac{\mathrm{d}\lambda_m}{\mathrm{d}k}(m = \tfrac{1}{2}k) = \tfrac{1}{2}k(2-k^2),$$

$$\beta = \frac{1}{2}\frac{\mathrm{d}^2\lambda_m}{\mathrm{d}k^2}(m = \tfrac{1}{2}k) = \tfrac{1}{2}(2-3k^2) < 0$$

are expansions of the primary growth rate near $\frac{1}{2}k$. Since $|A_k|^2$ can be obtained from (9*b*), one can easily derive from (24) that $d_{\frac{1}{2}-\epsilon} < d_{\frac{1}{2}}$ provided $|A_k|$ is larger than the critical value

$$|A_k|(k_c) = \tfrac{1}{8}\{\beta(k_c) + [k_c^2\beta^2(k_c) + 4\alpha^2(k_c)]^{\frac{1}{2}}\}. \tag{26}$$

A leading-order estimate of $|A_k|(k_c)$ in (26) can be obtained by expanding it about $k_c \sim 1$:

$$|A_k|(k_c) = 0.077. \tag{27}$$

Near the neutral curve, expansion of the fundamental amplitude (9*b*) about the neutral curve $k = 1$ yields

$$|A_k|^2 \sim \tfrac{3}{2}(1-k). \tag{28}$$

Combining (27) and (28), one obtains an estimate of the critical normalized wavenumber below which the subharmonic instability is the dominant streamwise secondary instability:

$$k_c \sim 0.9960, \tag{29}$$

which is in good agreement with the exact value of $k_c = 0.9952$ from our numerical stability analysis. Consequently, there is only a small interval below the neutral curve where the secondary sideband instability dominates the subharmonic instability. For most of the nearly neutral stationary waves of the γ_1 family with wavenumber k, the dominant secondary instability is the subharmonic instability whose growth rate can be estimated by combining (25) and (9*b*):

$$d_{\frac{1}{2}} = k^2\left\{\frac{187k^4 - 218k^2 + 40}{80k^2 - 32} + [(4k^2-1)(1-k^2)]^{\frac{1}{2}}\right\}. \tag{30}$$

At the neutral curve, $k = 1$, (30) yields the limiting subharmonic secondary growth rate of (18). It is also clear that, near the neutral curve, this subharmonic instability is a static one. In figure 5, we compare the above theory to our numerical Floquet stability results on the near-neutral γ_1 waves of the KS equation with respect to the secondary disturbance $\mathrm{e}^{\mathrm{i}k(1+\nu)X + \mathrm{i}k\hat{\beta}Z + dt}$ where $\nu = \frac{1}{2}$ corresponds to the subharmonic instability, $\nu < \frac{1}{2}$ the sideband instability, $\hat{\beta}$ the normalized transverse wavenumber and d the complex secondary growth rate. The above theory corresponds to two-dimensional secondary stability with $\hat{\beta} = 0$ but both the two-dimensional and three-dimensional dominant secondary modes and their secondary growth rates are depicted in figure 5. Details of our numerical formulation can be found in our earlier papers (Chang *et al.* 1993*a*, *b*). As is consistent with our prediction, the sideband instability is the dominant secondary instability for $k \in (0.9952, 1.0)$. At the neutral curve, the dominant sideband interval ν is in exact agreement with m_0 of (16). The sideband instability is replaced by

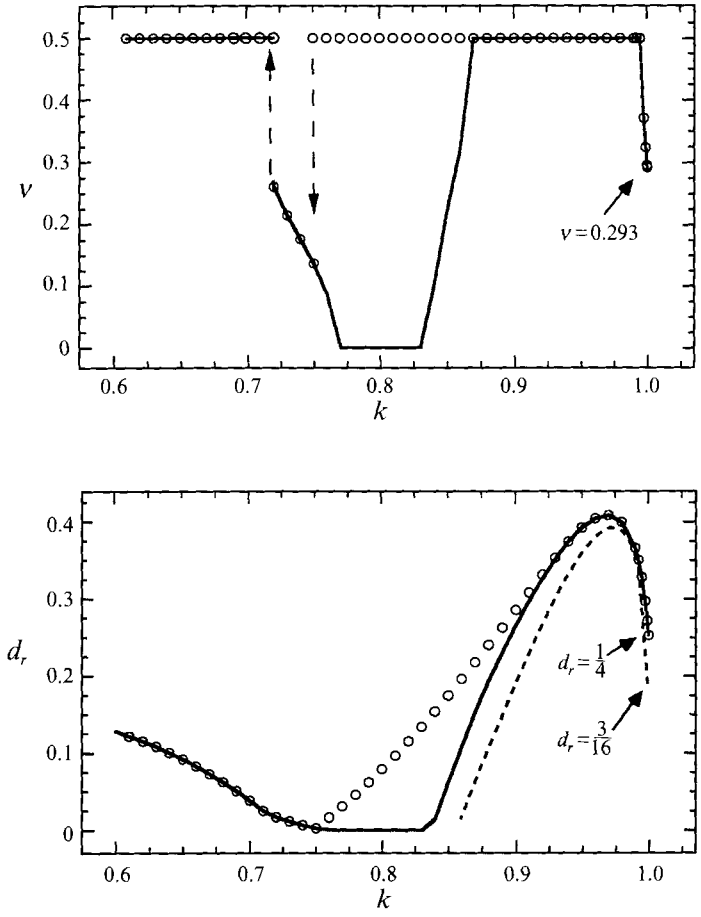

FIGURE 5. The real part of the dominant secondary two-dimensional (solid line) and three-dimensional (circles) growth rate d_r and streamwise wavenumber ν of the KS equation. The theoretical prediction $d_{\frac{1}{2}}$ of (30) is also shown as the broken line.

the subharmonic instability for lower k values and larger wave amplitudes. The estimated static subharmonic growth rate $d_{\frac{1}{2}}$ of (30), which approaches $\frac{3}{16}$ at $k = 1$, is also shown to be in good agreement with the numerical values for the subharmonic growth near $k = 1$ although the sideband instability dominates at exactly the neutral curve with the growth rate of $\frac{1}{4}$ as predicted in (17). Far below the neutral curve, where our weakly nonlinear theory would not apply, our numerical result shows that there is a band of KS stationary waves at $k \in (0.77, 0.84)$ that is stable to all two-dimensional streamwise disturbances. This stable band was first reported by Nepomnyaschy (1974*b*). Within this band, the most unstable streamwise disturbance is the sideband instability although it is not sufficient to destabilize the fundamental.

Having established that the sideband and subharmonic instabilities are the dominant streamwise instabilities for the fundamental saturated waves of the KS equation near the neutral curve and that, except for a small region near the neutral curve, the subharmonic instability dominates, we hence analyse the effect of transverse variation on the dominant subharmonic secondary instability. As shown in figure 4, transverse variation is stabilizing in the primary instability but this is different in the secondary instability owing to the nonlinear interaction with the fundamental. Because of the

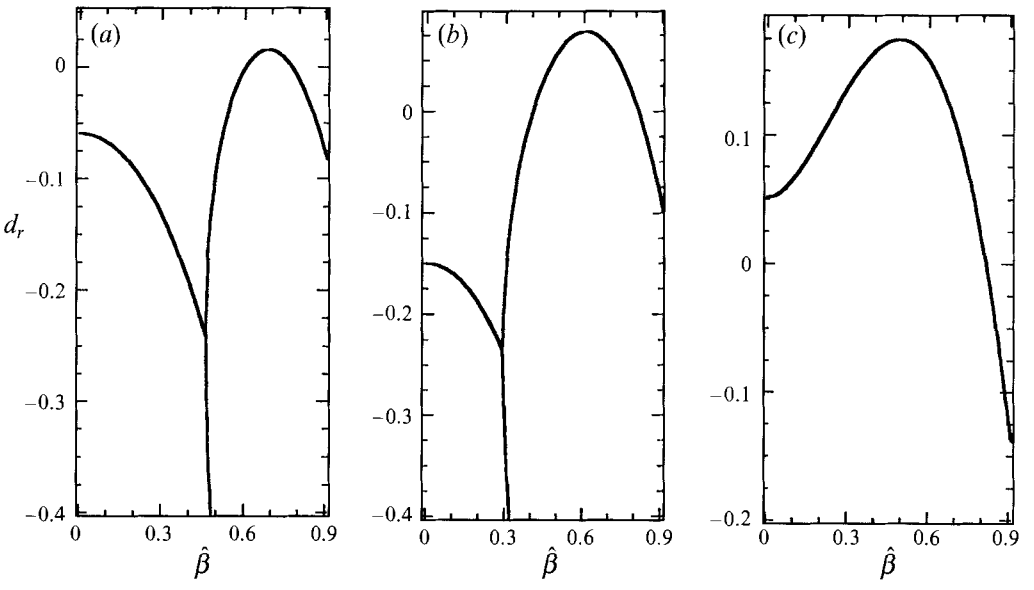

FIGURE 6. The KS secondary growth rate of the mode $d(\nu = \frac{1}{2}, \beta)$ as a function of the normalized transverse wavenumber $\hat{\beta} = \beta/k$. A fastest-growing transverse wave number β_m is evident and the instability at this dominant three-dimensional disturbance is static for the k values indicated. (*a*) $k = 0.75$; (*b*) $k = 0.80$; (*c*) $k = 0.85$.

translational invariance of the KS equation, in fact of the full equation, in the transverse direction, the contribution of transverse variation to both primary and secondary instabilities must vanish exactly at zero transverse wavenumber. This implies that, if the transverse variation is destabilizing, it is most likely a long-wave transverse instability which emanates from the zero-wavenumber limit. This long-wave approximation allows us to study three-dimensional secondary instability with a simple extension of the two-dimensional secondary stability theory for the KS equation. For long transverse variation ($\beta \ll 1$), all the nonlinear interaction coefficients remain identical to the two-dimensional ones and only the linear primary growth rates need to be adjusted to include transverse variation,

$$\lambda_{k/2} \sim (\tfrac{1}{2}k)^2 - [(\tfrac{1}{2}k^2) + \beta^2]^2, \tag{31}$$

where β is the transverse wavenumber of the primary disturbance. Expanding in β, it can be easily shown from (23) that the dominant three-dimensional secondary instabilities have growth rates

$$d_{\frac{1}{2},\beta} \sim d_{\frac{1}{2}} + \frac{-121k^6 + 140k^4 - 28k^2}{2(5k^2-2)^2}\beta^2 + \frac{67k^6 - 90k^4 - 12k^2 + 8}{(5k^2-2)^3}\beta^4, \tag{32}$$

where $d_{\frac{1}{2}}$ corresponds to the streamwise subharmonic growth rate of (30). It is clear from (32) that transverse variation enhances the instability of the streamwise subharmonic instability for $k < k_\beta = 0.949$ with a zero critical transverse wavenumber. This secondary excitation of three-dimensional waves involves the oblique-wave triad

$$\{(k, 0), (k/2, \beta_m), (-k/2, \beta_m)\}, \tag{33}$$

where β_m is the most unstable oblique mode, which can be estimated from (32) to be

$$\beta_m \sim 1.76(k_\beta - k)^{\frac{1}{2}} \tag{34}$$

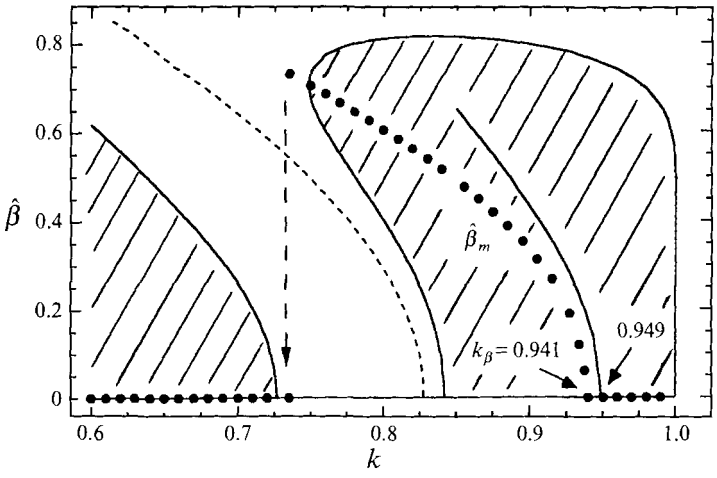

FIGURE 7. The unstable $\hat{\beta}$ range (shaded region) and the fastest-growing $\hat{\beta}$ mode, $\hat{\beta}_m$, of the secondary instability of the KS γ_1 wave. The solid line is the analytical estimate from (34). Three-dimensional secondary disturbance is more unstable than two-dimensional ones for $k < 0.94$. All instabilities to the right of the dotted curve are static and the ones to the left oscillatory.

near k_β and which can be converted to the normalized secondary wavenumber $\hat{\beta}$ through division by k: $\hat{\beta}_m = \beta_m/k$.

The above theory yields the most important result that the secondary instability of near-neutral γ_1 waves preferentially excites three-dimensional disturbances provided that the streamwise wavenumber is a subharmonic one. This destabilization mechanism is so strong that it even obliterates the stable window with respect to two-dimensional disturbances as shown in figure 5. All stationary waves of γ_1 between $k \in (0.75, 0.995)$ are unstable to the oblique-wave triad of (33). It is this oblique-wave triad that generates the checkerboard strip in the middle of the herringbone pattern in figure 2(*a*). We have hence established the secondary transition scenario from the γ_1 waves depicted in figure 3(*a*). The secondary excitation of the transverse mode involves the β^4 term of (32) at smaller wavenumber k such that the most unstable transverse wavenumber β_m increases at lower k-values, evident from the numerical secondary growth rates of figures 6 and 7, as suggested by our analytical estimate (34) which is in agreement with the numerical values as shown in figure 7. (The exact value of k_β from figure 7 is 0.941, which is in excellent agreement with the predicted value of 0.949 from (32).) When the β^4 term is required for destabilization, as shown for $k = 0.75$ and 0.8 in figure 6(*a*, *b*), there is a band of stable transverse wavenumbers near zero. The two subharmonic eigenvalues may even become complex at low $\hat{\beta}$ but these complex transverse modes are always stable as shown in figure 7. We summarize the secondary excitation of three-dimensional disturbances by the near-neutral stationary waves of the KS equation in figures 8 and 9, where the numerically obtained wavenumbers of the dominant secondary instability are depicted. The oblique-wave triads of (33) are shown on top of the primary neutral curve of the KS equation in figure 9. We note that for fundamental wavenumbers below $k = 0.76$, including the fastest-growing linear mode $k_m = 1/\sqrt{2}$, a stable three-dimensional primary wave can actually be excited by the secondary triad mechanism!

Near criticality when the KS equation applies, the oblique-wave triad excitation is the only possible evolution from the window of fundamental waves stable to two-dimensional disturbances. This is no longer true at larger δ where our earlier analysis

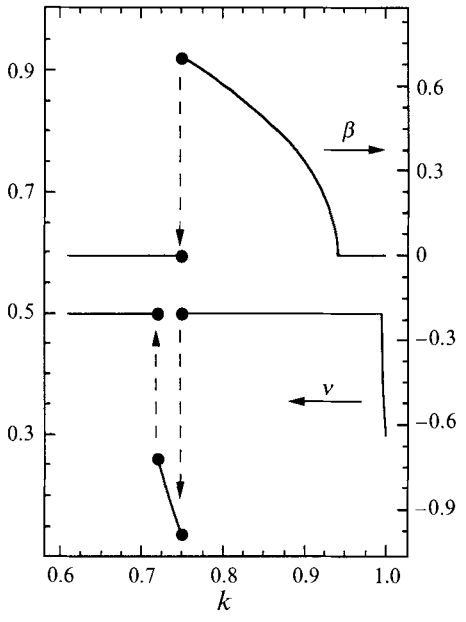

FIGURE 8. The wavenumbers of the dominant three-dimensional secondary disturbance of the KS γ_1 waves.

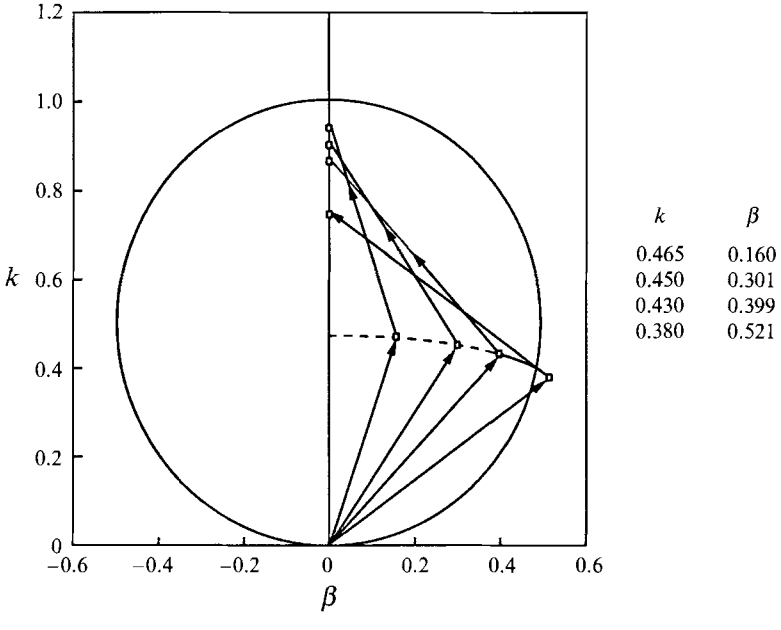

FIGURE 9. The oblique-wave triad excited by the KS γ_1 waves with wavenumber k. For $k < 0.76$, stable primary oblique waves outside the primary neutral curve are destabilized.

(Chang *et al.* 1993*a*) shows that some of the γ_2 waves are stable to two-dimensional disturbances. The second scenario, in figure 3(*b*), is then possible and transverse variation may be triggered from the γ_2 waves. We give a more detailed version of our numerical analysis of the stability of γ_1 and γ_2 waves for the boundary-layer equation for finite $\delta = 0.05$ in figure 10 and table 1. The secondary growth rate of the γ_1 family

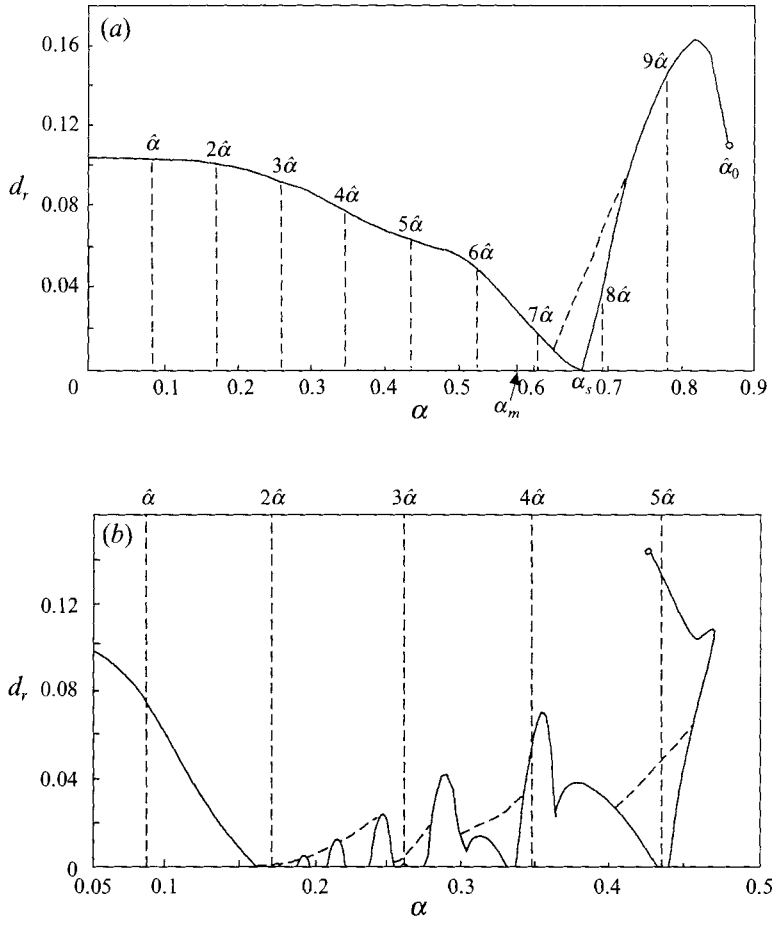

FIGURE 10. The secondary growth rates of (*a*) the γ_1 and (*b*) γ_2 waves of the boundary-layer equation. The fastest-growing linear mode at α_m, the least-unstable γ_1 wave at α_s and the wavenumber unit $\hat{\alpha} = \alpha_0/10$ and its harmonic are also shown. The solid lines are the two-dimensional growth rate while the dotted lines are for the three-dimensional growth rates.

	γ_1 family				γ_2 family			
Wavenumber	d_r	$d_r/\alpha c_i^{max}$	ν	β	d_r	$d_r/\alpha c_i^{max}$	ν	β
$\hat{\alpha} = 0.0866$	0.1078	0.991	0.0113	0	0.0751	0.690	0.5	0
$2\hat{\alpha} = 0.1732$	0.0982	0.903	0.0345	0	3.09×10^{-4}	0.003	0.5	0.005
$3\hat{\alpha} = 0.2598$	0.091	0.836	0.0305	0	1.17×10^{-3}	0.011	0.223	0.05
$4\hat{\alpha} = 0.3464$	0.0764	0.702	0.1051	0	5.23×10^{-2}	0.481	0.5	0
$5\hat{\alpha} = 0.4330$	0.0631	0.580	0.3011	0	4.15×10^{-2}	0.378	0.073	0.4
$6\hat{\alpha} = 0.5196$	0.0503	0.462	0.4737	0				
$7\hat{\alpha} = 0.6062$	0.0182	0.167	0.2895	0				
$8\hat{\alpha} = 0.6928$	0.0304	0.335	0.5	0.4				
$9\hat{\alpha} = 0.7794$	0.141	1.296	0.5	0				

TABLE 1. The secondary growth rate of the dominant three-dimensional disturbances at $\delta = 0.05$. The primary growth rate αc_i^{max} is 0.11 under this condition.

is essentially an extension of the KS result in figure 5. The window with waves stable to two-dimensional disturbances has now reduced to a small neighbourhood around $\alpha_s = 0.67$ at $\delta = 0.05$ which is shorter than the fastest growing linear mode at $\alpha_m = 0.578$. The dominant secondary instability of the $8\hat{\alpha}$ mode, which is closest to the stable window around α_s, is the oblique wave triad of (33) with β_m close to 0.4 (see table 1). The stability of the γ_2 waves is quite different, however. There are discrete intervals that are stable to two-dimensional disturbances. Waves within these intervals are unstable to three-dimensional disturbances, however, and from table 1 the dominant secondary instabilities for these waves are both the subharmonic triads of (33) and the sideband oblique-wave triad

$$\{(k, 0), (\tilde{k}, \beta), (\tilde{k}, -\beta)\}, \tag{35}$$

with $\beta \ll 1$ and $k \sim \tilde{k}$. With the sideband triad, the streamwise variation has almost the same wavelength as the stationary wave ($k \sim \tilde{k}$) and one hence sees only a long-wave envelope modulation and little change in the streamwise wave profile. The subharmonic triad also introduces only disturbances in the streamwise direction that are much smaller in amplitude than the γ_2 stationary waves of figure 1. There is hence little distortion of the streamwise wave profile by these two instabilities. However, since the stationary waves are two-dimensional with translational invariance in the transverse direction, the translational variation introduced by both three-dimensional disturbances is very apparent. This then suggests that the three-dimensional waves generated by the γ_2 waves are triggered by the transverse 'phase instability' shown in figure 2. Instead of the checkerboard pattern with pinching and phase shift, one expects mostly transverse modulation of the crests. In this scenario which occurs when there is very little transverse content in the noise, there would be four distinct wave regimes downstream from the feed, the inception region I, region II with slow γ_1 waves of wavenumber α_s, region III with faster and longer γ_2 waves and region IV with three-dimensional waves triggered by the γ_2 waves (see Chang 1994). Finally, we also note from table 1 that the secondary growth rate d is typically much smaller than the primary growth rate αc_i^{max}. This is especially true for the γ_2 waves which can have growth rates two orders of magnitude smaller than the primary one. This implies that the transition length for the secondary transition is far longer than the primary one. These transitions will be verified numerically in the next section.

4. Numerical experiment on wave transitions

To establish the two transition scenarios to three-dimensional patterns in figure 3 suggested by our secondary stability theory, we carry out a numerical study of wave evolution described by the boundary-layer equation (2) with periodic boundary conditions in x and z. The numerical approach is similar to our earlier two-dimensional evolution study (Chang *et al.* 1993*a*) with Fourier expansions in x and z and a second-order polynomial expansion in the y-direction within each domain of a seven-domain decomposition (Chang *et al.* 1993*b*). However, owing to the much larger computational and memory capacity required for the three-dimensional problem, we can only include 24 Fourier modes in the x-direction and 12 modes in the z-direction with the same unit wavenumber. The domain length in x is chosen such that exactly 10 streamwise x Fourier modes lie within the neutral curve as shown in figure 10, namely the unit wavenumber $\hat{\alpha}$ is one-tenth the neutral wavenumber α_0. The domain width in z is also of the same length so that the domain is exactly a square. The integration of time uses a fourth-order Runge–Kutta scheme. All integrations are done for $\delta = 0.05$,

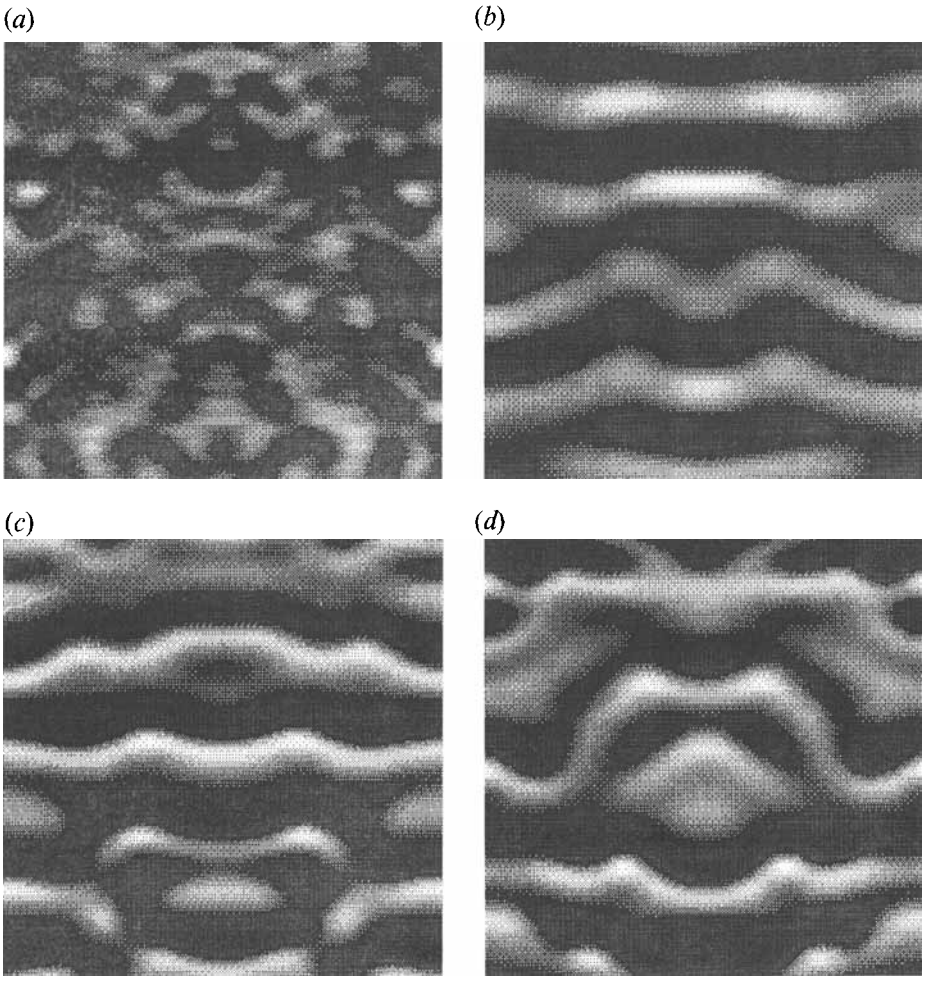

FIGURE 11. Interfacial height $h(x, z, t)$ at $t = 0$, 30, 70 and 100 (a–d). The crests are represented by the light strips. Primary filtering of transverse variation and the subsequent secondary excitation by the triad checkerboard pattern is evident.

corresponding to water with $\gamma = 2850$ and $R = 5.693$. At this condition the Nusselt film thickness is $h_N = 0.1313$ mm, the average velocity $\langle u \rangle = 4.944$ cm s^{-1} and the fastest growing linear mode at $\alpha_m = 0.5781$ in figure 10 corresponds to a wavelength of 1.083 cm. The square domain is then 7.23 cm in width and length.

In figure 11, we depict the interfacial height evolution with an initial condition that approaches white noise. The amplitudes of all modes in the unstable region are identical at 0.001 while their relative phases are determined from a random number generator. As seen from the evolution shown in figure 11, the primary instability filters the three-dimensional modes such that by $t = 30$, the waves are almost two-dimensional with only a slight transverse variation. About six or seven crests are observed at this stage, which are integer multiples of $\hat{\alpha}$ very close to the fastest-growing linear mode at α_m in figure 10. The wave profiles of these waves resemble the γ_1 waves. From figure 10, it is evident that $6\hat{\alpha}$ or $7\hat{\alpha}$ is also close to the least-unstable γ_1 wave at α_s. Consequently, within the coarse resolution we have here, we do not observe the wave compression from α_m to α_s seen in our more accurate two-dimensional simulation (Chang *et al.*

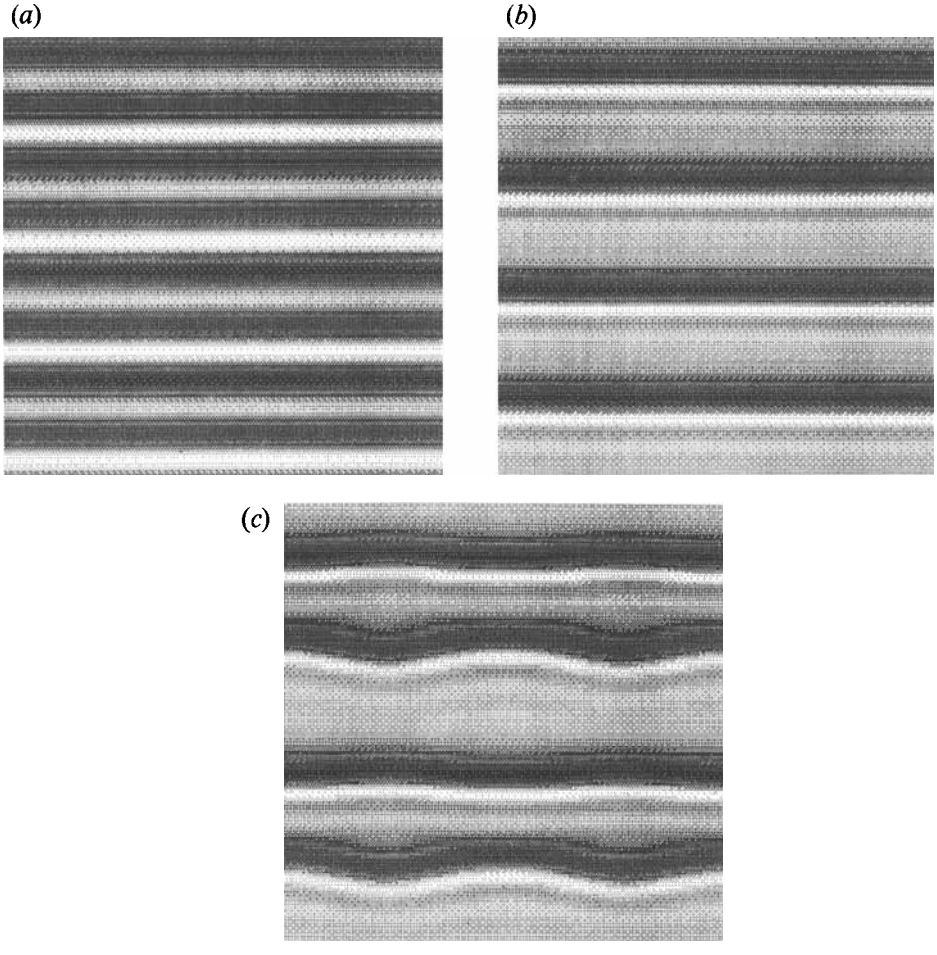

FIGURE 12. The $\gamma_1 \to \gamma_2 \to$ phase instability transition from our numerical integration for $t = 50$, 100, 250 (*a–c*). The streamwise y- and transverse x-directions in these diagrams both have dimensions ten times the neutral wavelength, $10 \times 2\pi/\alpha_0 = 2\pi/\hat{\alpha}$.

1993*a*). A transverse variation is triggered rapidly at this point with crest pinching clearly evident by $t = 70$ as the oblique-wave triad of (33) manifests itself. The checkerboard pattern in the middle of the herringbone in figure 2(*a*) is evident by $t = 100$. The streamwise subharmonic mode of the triad has effectively reduced the number of crests by half. Since our periodic boundary conditions in z cannot approximate the wall boundary effects, the two flanks of the herringbone clearly cannot appear. The checkerboard pattern appears to be non-stationary but owing to our periodic boundary conditions, downstream evolution beyond the triggering of the checkerboard pattern on a real film is probably not properly modelled here.

In figure 12, we simulate an evolution from an almost two-dimensional initial condition. Since three-dimensional modes cannot be excited if they are initially zero, some amount must be present for any transverse variation to develop subsequently. The initial conditions $h(8,0) = 0.2$, $h(m \neq 8, 0) = 0.01$, $h(8,1) = 0.003$ and $h(m \neq 8, n \neq 0, 1) = 0$ are used here where the indices m and n denote the harmonics of the unit wavenumbers $\hat{\alpha}$ in x and z, respectively. From figure 12 and the

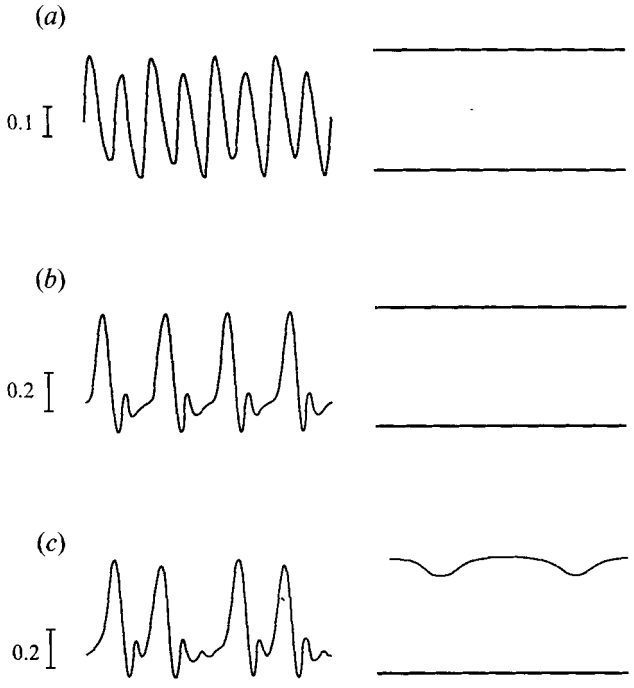

FIGURE 13. Cross-sections of the wave profile $h(x, z, t)$ at half the width and half the length of the three snapshots in figure 12. The width for both profiles is $2\pi/\hat{\alpha} = 72.55$ and the vertical scales are shown. The γ_2 waves are clearly evident.

wave profiles of figure 13, it is evident that the waves remain nearly two-dimensional as they evolve from a γ_1 wave near α_s with 8 crests to a γ_2 wave with a total of four crests as the $8\hat{\alpha}$ mode is unstable to a subharmonic two-dimensional disturbance as seen in table 1 and figure 10. The subharmonic instability of the γ_1 wave is clearly evident in figure 13 at $t = 50$ and the approach to a solitary wave like γ_2 wave of figure 1 is also apparent by $t = 100$. The γ_2 wave at $4\hat{\alpha}$ then triggers a crest-modulating phase instability as predicted in figure 3. It is interesting to note that the wave profiles in x still resemble the γ_2 solitary waves in figure 13 even after significant crest modulation has developed. The identical initial condition with the exception of a stronger three-dimensional content, $h(8, 1) = 0.01$, shows a dramatically different transition to the checkerboard pattern from the γ_1 wave without ever approaching the γ_2 waves, as shown in figure 14. We measure the two- and three-dimensional contents at any time by

$$I_{2D} = \frac{\sum_m |h(m, o)|}{\sum_m \sum_n |h(m, n)|}, \quad I_{3D} = 1 - I_{2D}, \tag{36}$$

and it can be seen from figure 15 that the triggering of the checkerboard pattern in figure 14 is extremely rapid at $t = 150$ in spite of the low secondary growth rate shown in table 1. This suggests a nonlinear acceleration process during the excitation of the three-dimensional patterns.

In an effort to simulate periodic forcing experiments, we have also carried out a series of numerical experiments with $h(m, 0) = 0.05$, where m is a specific integer, and $h(l, n) = \epsilon$ for $l \neq m$ and $n \neq 0$ with $\epsilon = 2 \times 10^{-6}$ and 10^{-5}. For $m < 5$, corresponding to $\alpha < \alpha_s$ as shown in figure 10, the γ_2 wave is always selected first without approaching a γ_1 wave. For $m > 5$, a γ_1 wave is first approached before a γ_2 wave with half the

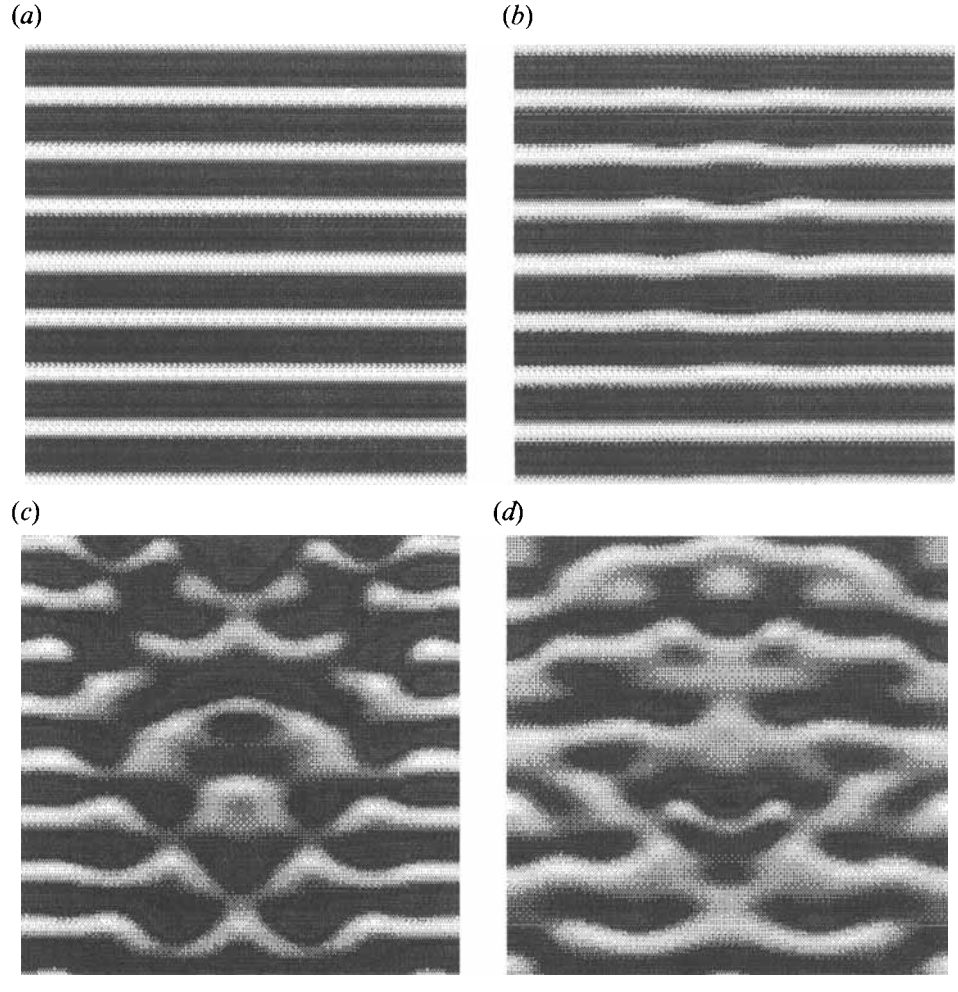

FIGURE 14. The $\gamma_1 \rightarrow$ checkerboard transition with more transverse content at $t = 0$, 70, 150, 200 (*a–d*).

wavenumber is selected. This is followed by the phase instability transition to three-dimensional patterns similar to the transitions in figures 12 and 13. If we define the transition time T_{3D} to three-dimensional patterns as when I_{3D} exceeds 0.2, our numerical experiments for periodic forcing are summarized in figure 16 where the transition length in cm is also shown. The two maxima at $m = 3$ and 7 correspond to the maximum secondary three-dimensional growth rates of the γ_1 and γ_2 waves in figure 10. These maxima should be observable in a sufficiently long channel.

5. Summary and conclusions

The secondary transitions on a falling film are easier to decipher than other hydrodynamic instabilities because of the formation of long-life two-dimensional stationary waves in the secondary and tertiary transitions. We can hence predict the next transition by constructing or estimating these stationary waves and studying their stability. We have used this approach to understand how transverse variation is triggered by secondary and tertiary instabilities of the stationary waves even though

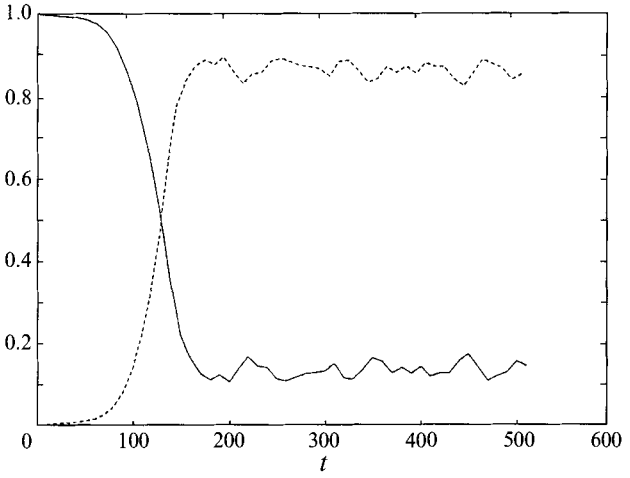

FIGURE 15. The explosive excitation of the checkerboard pattern in figure 14 at $T_{3D} \sim 150$: solid line (I_{2D}) and dotted line (I_{3D}).

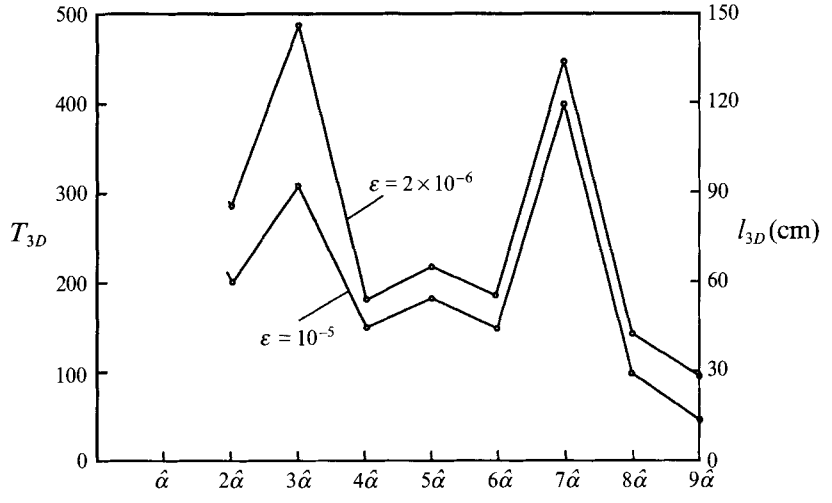

FIGURE 16. The three-dimensional transition time and length for periodic forcing. The transition time T_{3D} is defined as the time when I_{3D}, the fraction of three-dimensional Fourier wave content, exceeds 0.2. The transition length is defined as the product of the phase speed of the fastest-growing primary disturbance with T_{3D}. The parameter ϵ measures the amplitude of the initial two-dimensional disturbance.

they are suppressed by the primary instability. The two possible evolution scenarios to the checkerboard pattern and the modulated crest pattern are confirmed by our numerical experiments. Unfortunately, the three-dimensional patterns are extremely non-stationary as one would expect from experimental observation of the developed three-dimensional interfacial turbulence downstream. The non-stationary dynamics of the checkerboard pattern and the phase instability hence dominates this turbulence. It is quite possible that this subsequent non-stationary dynamics evolves around unstable three-dimensional stationary waves and the construction of the latter would be a worthwhile endeavour. In particular, scallop-shaped three-dimensional solitary waves have been observed to play some role in the eventual turbulent state. Such solutions

will be presented in a subsequent manuscript. However, full understanding of three-dimensional evolution can only be achieved without invoking spatial periodicity due to its non-stationary nature and sensitivity to inlet noise. This final breakthrough would then complete the delination of the intriguing hydrodynamic transitions to turbulence on a falling film.

This work is supported by DOE under the Engineering Research Program.

REFERENCES

ALEKSEENKO, S. V., NAKORYAKOV, V. E. & POKUSAEV, B. G. 1985 Wave formation on a vertical falling liquid film. *AIChE J.* **31**, 1446–1460.

BENNEY, B. J. 1966 Long waves in liquid films. *J. Math. Phys.* **45**, 1150–1155.

CHANG, H.-C. 1994 Wave evolution on a falling film. *Ann. Rev. Fluid Mech.* **26**, 103–136.

CHANG, H.-C., DEMEKHIN, E. A. & KOPELEVICH, D. I. 1993*a* Nonlinear evolution of waves on a falling film. *J. Fluid Mech.* **250**, 433–480.

CHANG, H.-C., DEMEKHIN, E. A. & KOPELEVICH, D. I. 1993*b* Laminarizing effects of dispersion in an active-dissipative nonlinear medium. *Physica* D **63**, 299–320.

CHANG, H.-C., DEMEKHIN, E. A. & KOPELEVICH, D. I. 1993*c* Construction of stationary waves on a falling film. *Comput. Fluid Dyn.* **11**, 313–322.

CHEN, C. C., LAHBABI, A., CHANG, H.-C. & KELLEY, R. E. 1991 Spanwise pairing of finite-amplitude longitudinal vortex rolls in inclined free-convection boundary layer. *J. Fluid Mech.* **231**, 73–111.

CHENG, M. & CHANG, H.-C. 1990 A generalized sideband stability theory via center manifold projection. *Phys. Fluids* A **2**, 1364–1379.

CHENG, M. & CHANG, H.-C. 1992 Subharmonic instabilities of finite-amplitude monochromatic waves. *Phys. Fluids* A **4**, 505–523.

DEMEKHIN, E. A., KAPLAN, M. A. & SHKADOV, V. YA. 1987 Mathematical models of the theory of viscous liquid films. *Izv. Akad. Nauk SSSR, Mekh Zhidk. i Guza* **6**, 73–81.

JOO, S. W. & DAVIS, S. H. 1992 Instabilities of three-dimensional viscous falling films. *J. Fluid Mech.* **242**, 529–547.

JOO, S. W., DAVIS, S. H. & BANKOFF, S. G. 1991 On falling film instabilities and wave breaking. *Phys. Fluids* A **3**, 231–232.

KURAMOTO, Y. 1984 *Chemical Oscillations, Waves and Turbulence*. Springer.

LIU, J., PAUL, J. D., BANILOWER, E. & GOLLUB, J. P. 1992 Film flow instabilities and spatio-temporal dynamics. In *Proc. First Experimental Chaos Conf.* (ed. S. Vohra, M. Spano, M. Schlesinger, L. M. Pecora & W. Ditto), pp. 225–239. World Scientific.

LIU, J., PAUL, J. D. & GOLLUB, J. P. 1993 Measurement of the primary instabilities of film flows. *J. Fluid Mech.* **220**, 69–101.

NEPOMNYASCHY, A. A. 1974*a* Stability of wave regimes in a film flowing down on inclined plane. *Izv. Akad. Nauk SSSR, Mekh. Zhidk i Gaza* **3**, 28–34.

NEPOMNYASCHY, A. A. 1974*b* Three-dimensional spatially-periodic motions in liquid films flowing down a vertical plane. *Hydrodynamics* (*Russian*) *Perm* **7**, 43–52.

ORSZAG, S. A. & KELLS, L. C. 1980 Transition to turbulence in plane Poiseuille and plane Couette flow. *J. Fluid Mech.* **96**, 159–205.

PROKOPIOU, TH. CHENG, M. & CHANG, H.-C. 1991 Long waves on inclined films at high Reynolds number. *J. Fluid Mech.* **222**, 665–691.

PUMIR, A., MANNEVILLE, P. & POMEAU, Y. 1983 On solitary waves running down an inclined plane. *J. Fluid Mech.* **135**, 529–547.

ROSENAU, P., ORON, A. & HYMAN, J. M. 1992 Bounded and unbounded patterns of the Benney equation. *Phys. Fluids* A **4**, 1102–1104.

SALAMON, T. R., ARMSTRONG, R. C. & BROWN, R. A. 1994 Traveling waves on vertical films: Numerical analysis by the finite element method. *Phys. Fluids* (in press).

THOMAS, F. O. 1990 An experimental investigation into the role of simultaneous amplitude and phase modulation in the transition of a planar jet. *Phys. Fluid* A **2**, 553–570.